Optical spectroscopy of charged excitons in single quantum dot photodiodes

M. Baier, F. Findeis, A. Zrenner, M. Bichler, and G. Abstreiter
Walter Schottky Institut, Technische Universität München, Am Coulombwall, 85738 Garching, Germany
(Received 28 March 2001; published 26 October 2001)

By means of photoluminescence spectroscopy we compare the bias dependent emissions of single quantum dots which are embedded in two differently designed photodiode structures. Controlled single-electron charging allows to identify neutral, single- and double-charged excitons in the optical spectra of both samples. The strength of the tunneling coupling between the quantum dots and the diode's *n* region is found to have a strong influence on the observed spectral features—in particular, the parallel appearance of emission lines resulting from the radiative decay of differently charged quantum dot states is suppressed in case of strong tunneling interaction.

DOI: 10.1103/PhysRevB.64.195326 PACS number(s): 73.21.−b, 78.55.Cr, 78.66.−w

In recent years, the investigation of self-assembled semiconductor quantum dots (QDs) has developed into one of the most important subjects in low-dimensional semiconductor physics. Neutral multiexciton states in QDs have been investigated by photoluminescence (PL) spectroscopy and corresponding theoretical investigations.[1–7] Charged exciton states were first observed in quantum-well structures.[8] In QDs charged exciton states have been studied in inhomogeneously broadened ensembles by PL measurements[9] as well as in interband transmission experiments,[10] most recently also in single optically-tunable QDs,[11,12] as well as in electrically tunable quantum rings.[13] Apart from that, we have lately reported on our investigation of neutral and charged excitons in single QDs, realized by means of magneto-PL experiments[14] and by photocurrent experiments[15] on QDs that were integrated into photodiode structures. So far the main focus of this work was concentrated on determining charged exciton binding energies both via experiment and theoretical model calculations.

In the present paper we take a closer look at the interaction of the QDs with their environment within a photodiode. In particular, we demonstrate how differences in the tunneling coupling between QDs and the electron reservoir in the diode's *n* region affect the bias dependent photoluminescence spectra. The understanding of this topic is important with regard to future experiments and applications, where the controlled tuning of absorption and emission energies by single electron charging in QDs will play an important role.

For controlled charging of individual QDs two different electric field tunable *n-i* structures were grown by molecular beam epitaxy. In the first sample $In_{0.5}Ga_{0.5}As$ QDs are embedded in an *i*-GaAs layer 40 nm above an *n*-doped GaAs layer (5×10^{-18}), which acts as a back contact. The growth of the QDs is followed by 270 nm *i*-GaAs, a 40-nm-thick $Al_{0.3}Ga_{0.7}As$ blocking layer, and a 10 nm *i*-GaAs cap layer. A 5-nm-thick Ti layer is used as a semitransparent Schottky gate. With respect to the distance between the *n*-GaAs layer and the QDs this sample is referred to as the 40 nm sample. In the second sample—the 20 nm sample—the width of the intrinsic region and the distance between the *n*-GaAs layer and the QDs is only half as wide. Both samples were processed as photodiodes combined with electron-beam-structured shadow masks with apertures ranging from 200 nm to 500 nm. A schematic cross-section representing both samples is shown in Fig. 1. Additionally the band diagrams of the samples are displayed: Overviews and details of the energy band structure are depicted in Fig. 2(a) and Fig. 2(b) for the 20 nm and the 40 nm sample.

The occupation of the QDs can be controlled by varying the external bias voltage V_B between the Schottky gate and the back contact. For increasing V_B the band flattens and the QD electron levels are subsequently shifted below the Fermi energy E_F of the *n*-GaAs region. This results in a step-by-step occupation of the QD with electrons: First, the QD *s* shell is brought below E_F. As a consequence the *s* shell is occupied with one electron via tunneling between the *n*-GaAs region and the QDs. The voltage for which the second s-shell electron state is occupied is larger. This is due to the fact that a Coulomb charging energy of about 20 meV has to be taken into account for the second electron.[16] Due to the same reason and additionally due to the confinement energies of the higher shells also the voltages for which the QD is occupied with three, four and more electrons are shifted to higher V_B values.

In the PL experiments which were performed on the samples, excitons were optically generated at low rate by means of non-resonant excitation with a HeNe laser (632.8 nm). Together with the V_B-induced electrons these excitons form the neutral, single-, and double-charged excitons X^0, X^{1-}, and X^{2-} in the QD. A 0.7 m Dilor spectrometer combined with a liquid-N_2-cooled charge-coupled device (CCD) camera was used for detection of the PL. The sample was mounted in a confocal low-temperature microscope.[17]

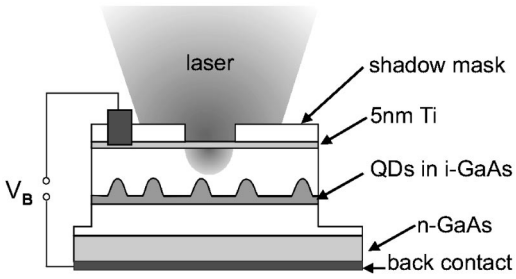

FIG. 1. Schematic sample structure: QDs integrated in a photodiode combined with a near-field shadow mask.

 ©2001 The American Physical Society

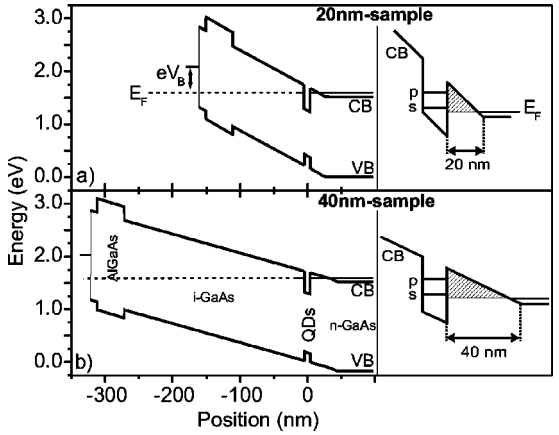

FIG. 2. Energy-band structure: Overview and detail of the conduction band close to the QDs for the (a) 20 nm sample and (b) 40 nm sample.

In the gray-scale plot of Fig. 3(a) PL spectra of a single QD are plotted versus the external bias voltage V_B. Figure 3(b) contains analogous data from two other QDs in the same sample in order to demonstrate the reproducibility of the experimental results. The observed emission lines result from *s*-shell transitions of the X^0, X^{1-}, and X^{2-} excitons. In the voltage range labeled as V_{PC} the QD is electrically neutral, but no PL is observed due to the comparably high electric field strength F. Under this condition carriers tunnel out of the QD rather than recombine radiatively. Within V_{PC} we have performed photocurrent measurements on the same QD.[15] Within V_0 the QD is still electrically neutral. The smaller electric field results in smaller tunneling losses and in a detectable emission of the sharp X^0 line in PL. Within V_1 the QD is occupied with one electrostatically induced electron. As a consequence the X^{1-} emission line appears 4.6 meV below the X^0 emission line. Within V_2 the occupation with the second electrostatically induced electron leads to X^{2-} emission, which is characterized by the appearance of two emission lines. These two lines result from the existence

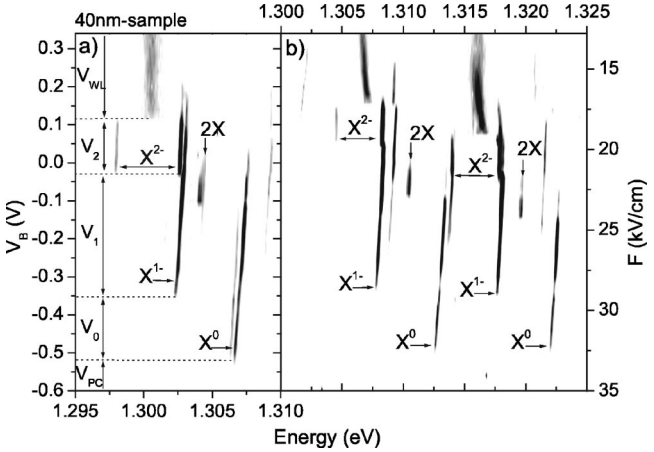

FIG. 3. 40 nm sample: (a) Gray-scale plot of the PL intensity as a function of the emission energy and the bias voltage V_B. Parallel emission of X^0 and X^{1-} as well as of X^{1-} and X^{2-} from a single QD can be observed. (b) Analogous data from two other QDs.

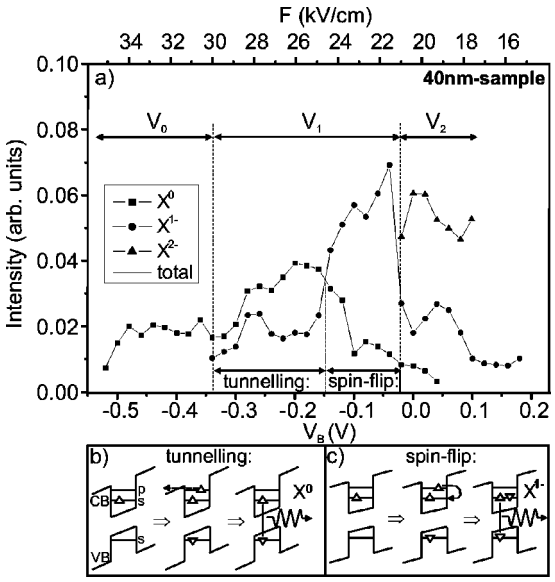

FIG. 4. 40 nm sample: (a) Bias-dependent X^0, X^{1-}, and X^{2-} emission intensities revealing a change from dominant X^0 to dominant X^{1-} emission at $V_B=-0.15$ V. (b) Tunneling process resulting in X^0 emission. (c) Spin-flip process resulting in X^{1-} emission.

of an energetically higher triplet and a lower singlet final state with regard to the *s*-shell and *p*-shell electron that remain in the QD after the X^{2-} decay. The two lines are separated by the corresponding *s*-*p* exchange energy K, which has a value of 4.6 meV for the investigated QD. Within V_{WL} only one broad emission line remains. This indicates the filling of wetting layer (WL) states with electrons. Here weakly confined electrons interact with the carriers in the QD causing a broadening of the detected *s*-shell decay. We have justified the assignment of the observed emission lines to the decay of the X^0, X^{1-}, and X^{2-} excitons by comparing theoretical calculations with the experimental results in an earlier publication.[14] The investigation of 14 different QDs resulted in an average value of 4.75 ± 0.43 meV for the X^{1-} binding energy and a value of $K=1.95\pm0.05$ meV for the *s*-*p* electron-electron exchange interaction. The standard deviations are attributed to variations in the confinement potentials, which result from size and shape fluctuations of the self-assembled QDs. The comparably small standard deviation for K suggests that the *s*-*p* exchange interaction is less influenced by the details of the confinement potential.

As mentioned before the QD is single-charged within V_1. Surprisingly however, not only the expected X^{1-} emission, but also X^0 emission is observed in this voltage range. Even within V_2 not only X^{2-} but also X^{1-} emission is observed. A more quantitative illustration of this aspect is provided in Fig. 4(a), where the integrated emission intensities are plotted versus V_B. The observed parallel emission results from the time-integrating character of the CCD measurements combined with the statistical occurrence of different emission processes. Within the V_1 voltage range, for example, there are two major processes resulting in X^0 emission.

First, a single photoexcited hole can be captured by the single charged QD. Consequently an X^0 is formed and X^0 emission follows. Second, there is the following scenario

involving a tunneling process: Due to the linear polarization of the excitation light, statistically every second exciton relaxing into the QD leads to a spin configuration where both electron spins are oriented in parallel. As a consequence the optically induced electron cannot relax down to the *s* shell due to Pauli blocking. Thus it temporarily remains in the *p* shell until it tunnels out of the QD. This process results in X^0 emission within V_1, it is illustrated in Fig. 4(b). In case of opposite spin orientation of the electrostatically induced electron with respect to the optically induced electron, both electrons can be accommodated in the *s* shell and a X^{1-} is formed, which eventually decays.

An important feature in Fig. 4(b) is the observed change from dominant X^0 emission to dominant X^{1-} emission which occurs at $V_B=-0.15$ V. This change can be explained as follows: The F dependent tunneling-time reaches such a large value for $V_B>-0.15$ V that Pauli-blocked *p*-shell electrons are more likely to relax down to the *s* shell by a spin-flip process than to tunnel out of the QD. Consequently the tunneling process illustrated in Fig. 4(b) is replaced by the spin-flip X^{1-} emission process which is illustrated in Fig. 4(c). Reversing all spins in the displayed processes corresponds to the emission of photons with opposite circular polarization. With regard to Zeeman components this will be of importance in the final part of this paper where magnetic field data will be discussed.

Note, that for X^0 emission within the voltage range V_1 as well as for X^{1-} emission within the voltage range V_2 the QD is in a nonequilibrium charging state prior to photon emission. In an electrostatic equilibrium situation there should be one more electron in the QD in both cases. Since the tunneling coupling between the *n*-GaAs region and the QD is rather weak in this sample, an electrostatic equilibrium situation in the QD can not be established before radiative emission takes place.

Further discussion of this aspect is based on the properties of the second sample—the 20 nm sample. In this sample the tunneling barrier between the *n*-GaAs region and the QDs is only half as wide as in the 40 nm sample. The influence of this difference on the tunneling probability for electrons tunneling through the barrier can be estimated on the basis of a one-dimensional WKB approach:[18] In this calculation the properties of the tunneling barriers in the two samples have to be taken into account (see the gray-shaded triangles in the righthand parts of Fig. 2). The width of the triangular barrier is 20 nm for the 20 nm sample and 40 nm for the 40 nm sample; it is basically independent of V_B. In Fig. 5 the tunneling probabilities of electrons tunneling through the 20 nm and the 40 nm barrier are plotted versus the barrier height, which is is proportional to V_B. As a first conclusion, the tunneling probability is always at least 10^4 times larger in the 20 nm sample. For the comparison of the two samples this finding is independent of more specific assumptions made for the barrier height. Still, the actual barrier heights for the V_1 voltage range can be estimated as follows: The voltage range V_1 is limited as follows: In the low-voltage limit, the QD is electrostatically charged with one electron, i.e., E_F is aligned with the *s* shell, which is about 130 meV below the confining GaAs conduction-band edge. In the high voltage

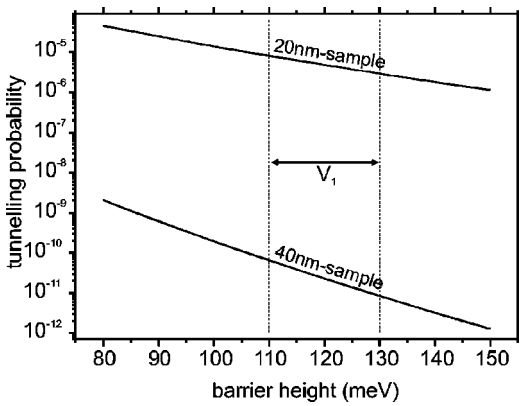

FIG. 5. Tunneling probabilities for electrons tunneling from the *n*-GaAs region into the QD versus the corresponding barrier height.

limit the QD is charged with the second electron. In this situation the QD vacant *s*-shell state is shifted to a 20 meV higher value due to the above-mentioned charging energy. In other words the height of the tunneling barrier is tuned from about 130 meV to about 110 meV within V_1.

Due to the enhancement of the tunneling probabilities in the 20 nm sample as compared to the 40 nm sample, nonequilibrium charging states have considerably smaller lifetimes in the 20 nm sample. This aspect is expected to lead to suppressed parallel emission of lines which are assigned to the decay of differently charged excitons in the 20 nm sample. This is nicely confirmed by the experimental results: Figure 6(a) contains the V_B-dependent PL spectra of the 20 nm sample. Similar to the 40 nm sample the series of X^0, X^{1-}, and X^{2-} emission lines is observed. In contrast to the 40 nm sample there is no parallel emission in the 20 nm sample. Again the spectral features are very well reproduced as can be seen from Figs. 6(b) and 6(c) where the emission of two other QDs in the 20 nm sample is displayed. In Fig. 7 the emission intensities of the 20 nm sample are plotted versus V_B. Similar to the 40 nm sample a trend to higher emission intensities for decreasing F can be observed. In

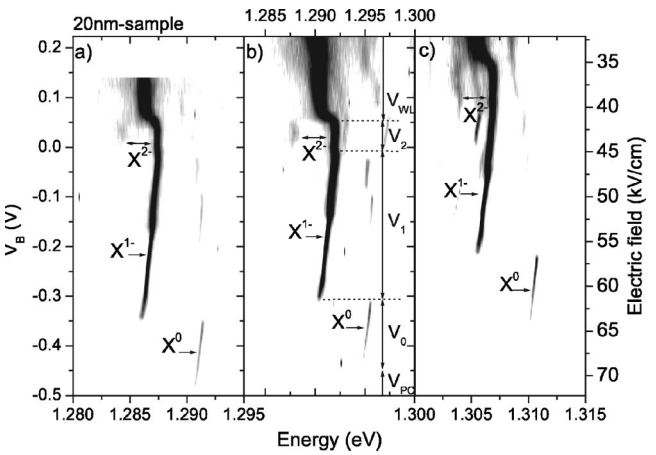

FIG. 6. 20 nm sample: (a) Gray-scale plot of the PL intensity as a function of the emission energy and the bias voltage V_B. No parallel emission can be observed. (b) and (c) Analogous data from two other QDs.

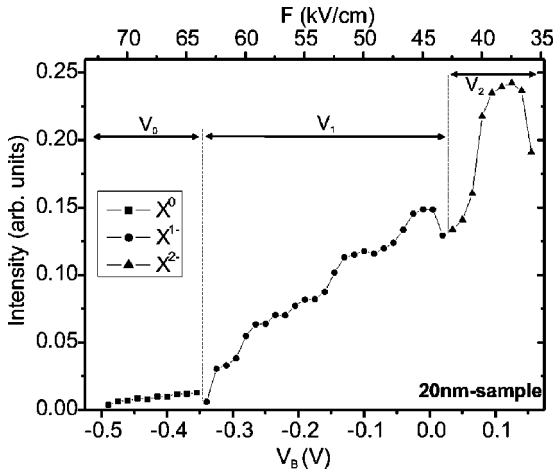

FIG. 7. 20 nm sample: Bias dependent emission intensities of the X^0, X^{1-}, and X^{2-} emission revealing a general increase of emission intensities with decreasing electric field.

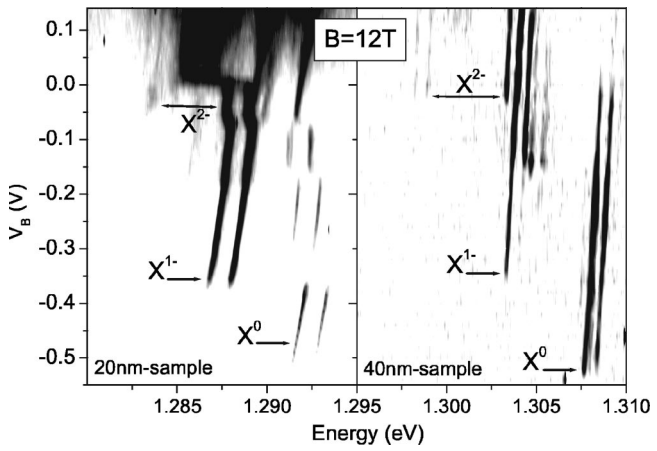

FIG. 8. $B=12$ T experiments: In both samples the emission lines split into two Zeeman components and diamagnetically shift to higher emission intensities. In the 40 nm sample a spin selective tunneling process results in the quenching of the high energy Zeeman component of the X^{1-} emission.

both samples this is due to the general decrease of tunneling losses for smaller electric fields.

As for the measurements that were performed on single electrically tunable quantum rings (QRs) by Warburton *et al.*[13] no parallel emission was observed. On the basis of our findings this is in good agreement with the fact, that QRs have comparably small confinement potentials and therefore also smaller tunneling barriers. This in turn leads to a tunneling coupling that is strong enough to suppress parallel emission.

All spectra of the 40 nm sample exhibit another characteristic emission line. This feature is assigned to the decay of a neutral biexciton ($2X$, see in Fig. 3). Its energetic position is about 3 meV below the X^0 emission line which is in good agreement with our findings from power-dependent single QD spectroscopy.[6] Apart from that, its V_B range perfectly corresponds to the part of the V_1 range where X^{1-} emission dominates; see Fig. 4(a). In this part of V_1 the statistical probability of the QD to be occupied with an X^{1-} is enhanced. Starting from this condition the negatively charged QD can capture a single hole by optical absorption followed by field ionization and drift within the spacer layer between the *n*-GaAs back contact and the QDs. This results in the formation of a $2X$ state, which eventually decays. In contrast, almost no 2X emission is observed at equally low excitation power in the 20 nm sample. Because of the reduced spacer layer thickness the capture of single holes is suppressed here in comparison to the 40 nm sample.

Let us finally take a look at experiments which were performed at a magnetic field strength of $B=12$ T. Figure 8 contains the obtained bias dependent PL spectra for both samples. In both cases the emission lines split into two Zeeman components and are diamagnetically shifted to higher emission energies. As for the 40 nm sample the higher-energy Zeeman component of the X^{1-} emission line is found to be quenched in the part of V_1 where the tunneling process displayed in Fig. 4(b) is dominant. This is due to the fact that the electrostatically induced *s*-shell electron, which is involved in the formation of the X^{1-}, is spin polarized at $B=12$ T—let us consider it to be spin-up oriented. Then an electron-spin-up/hole-spin-down exciton (bright exciton) relaxing into the QD always results in the tunneling process displayed in Fig. 4(b). Since the considered exciton spin configuration corresponds to the emission of one of the Zeeman components, the described mechanism results in its quenching. And even this finding is not observed in the 20 nm sample since the involved tunneling process is effectively compensated by electrons with suitable spin orientation (for this example spin-down) tunneling back into the QD from the *n*-GaAs region.

In summary, we have demonstrated bias controlled single electron charging by means of PL experiments on two differently designed single QD photodiodes. In particular, we have shown that the strength of the tunneling coupling between the QDs and the *n*-GaAs region of the samples has a strong influence on the observed bias dependent PL spectra: The parallel appearance of emission lines resulting from differently charged QD states is suppressed in case of strong coupling.

This work was financially supported by the DFG via SFB 348, by the BMBF via 01BM917.

[1] For a recent review, see A. Zrenner, J. Chem. Phys. **112**, 7790 (2000).
[2] E. Deckel *et al.*, Phys. Rev. Lett. **80**, 4991 (1998).
[3] L. Landin *et al.*, Science **280**, 262 (1998).
[4] P. Hawrylak, Phys. Rev. B **60**, 5597 (1999).
[5] U. Hohenester, F. Rossi, and E. Molinari, Solid State Commun. **111**, 187 (1999).
[6] F. Findeis, A. Zrenner, G. Böhm, and G. Abstreiter, Solid State Commun. **114**, 227 (2000).
[7] M. Bayer *et al.*, Nature (London) **405**, 923 (2000).

[8] K. Kheng *et al.*, Phys. Rev. Lett. **71**, 1752 (1993).
[9] K. H. Schmidt, G. Medeiros-Riberio, and P. M. Petroff, Phys. Rev. B **58**, 3597 (1998).
[10] R. J. Warburton *et al.*, Phys. Rev. Lett. **97**, 5282 (1997).
[11] A. Hartmann *et al.*, Phys. Rev. Lett. **84**, 5648 (2000).
[12] F. Finley *et al.*, Phys. Rev. B **63**, 073 307 (2001).
[13] R. J. Warburton *et al.*, Phys. Rev. Lett. **79**, 5282 (2000).
[14] F. Findeis *et al.*, Phys. Rev. B **63**, 121 309 (2001).
[15] F. Findeis *et al.*, Appl. Phys. Lett. **78**, 2958 (2001).
[16] H. Drexler *et al.*, Phys. Rev. Lett. **73**, 2252 (1994).
[17] A. Zrenner *et al.*, Physica B **256-258**, 300 (1998).
[18] F. Schwabel, *Quantenmechanik* (Springer-Verlag, Berlin, 1993).